Metamagnetic transition in single-crystal $Bi_4Cu_3V_2O_{14}$

H. D. Zhou,[1,*] E. S. Choi,[1] Y. J. Jo,[1] L. Balicas,[1] J. Lu,[1] L. L. Lumata,[1,2] R. R. Urbano,[1] P. L. Kuhns,[1] A. P. Reyes,[1] J. S. Brooks,[1,2] R. Stillwell,[1] S. W. Tozer,[1] C. R. Wiebe,[1,3] J. Whalen,[1] and T. Siegrist[1,4]

[1]*National High Magnetic Field Laboratory, Florida State University, Tallahassee, Florida 32306-4005, USA*

[2]*Department of Physics, Florida State University, Tallahassee, Florida 32306-3016, USA*

[3]*Department of Chemistry, University of Winnipeg, Winnipeg, Manitoba, Canada R3B 2E9*

[4]*Department of Chemical and Biomedical Engineering, Florida State University, Tallahassee, Florida 32310, USA*

(Received 12 April 2010; revised manuscript received 16 August 2010; published 31 August 2010)

We report on high magnetic field magnetization, magnetic torque, specific-heat, and ^{51}V NMR measurements on $Bi_4Cu_3V_2O_{14}$ single crystals, which display a characteristic chain structure along the crystallographic *a* axis. The system undergoes a magnetic phase transition below 5.5 K. For the magnetic field $H \| a$, the data reveal a metamagnetic transition from an antiferromagnetic (AFM) to a weak-ferromagnetic (WFM) state at $H_c \simeq 7.6$ T. Based on our results, the low-temperature magnetic phase diagram is determined. Furthermore, the magnetization measurements along with the NMR results suggest that the weak ferromagnetism along the *a* axis is possibly due to a canted AFM spin structure with two distinct magnetic sublattices.

DOI: 10.1103/PhysRevB.82.054435 PACS number(s): 75.50.−y, 75.30.Gw

I. INTRODUCTION

The copper-based oxides containing one-dimensional spin chain structure of Cu^{2+} ($3d^9$) have been one of the most active fields in condensed-matter physics due to the discovery of their various interesting magnetic behaviors. There are two categories of compounds: (i) the systems have a spin-singlet ground state with a finite spin gap due to their strong quantum spin fluctuation, such as $CuGeO_3$,[1] $BaCuSi_2O_6$,[2] $SrCu_2O_3$,[3,4] and $BaCu_2V_2O_8$.[5] (ii) The systems, such as $BaCu_2Si_2O_7$,[6] $CuSiO_3$,[7] $Cu_2V_2O_7$,[8] and $LiCuVO_4$,[9,10] undergo a magnetic ordering at low temperature due to weak interchain interactions. It is well known that applied magnetic fields on this category compounds *may indeed* induce metamagnetic transitions. For example, $BaCu_2Si_2O_7$ (Ref. 6) exhibits an interesting two-stage spin-flop transitions at 2 and 4.9 T, $CuSiO_3$ (Ref. 7) and $Cu_2V_2O_7$ (Ref. 8) both show a one-step spin-flop transition, and $LiCuVO_4$ (Ref. 11) shows indications of a magnetic phase structure change around 7.5 T.

$Bi_4Cu_3V_2O_{14}$ is another system with novel spin chain structure of Cu^{2+}, in which V^{5+} is nonmagnetic. Its crystal symmetry is triclinic $P\bar{1}$. The lattice constants are $a=5.3106(1)$ Å, $b=7.9019(2)$ Å, $c=8.0722(2)$ Å, $\alpha=74.038(2)°$, $\beta=90.597(2)°$, and $\gamma=70.417(2)°$. The structure of $Bi_4Cu_3V_2O_{14}$ can be described as $Cu_3V_2O_{12}$ chains separated by Bi_4O_2 chains along the *a* direction [Fig. 1(a)]. In each $Cu_3V_2O_{12}$ chain [Fig. 1(b)], the corner-sharing CuO_4 square planes form a Cu_3O_8 triple chain consisting of three nearly coplanar CuO_4 chains, and the outer two CuO_4 chains are corner sharing with VO_4 tetrahedra. If the CuO_4 units of the Cu_3O_8 triple chain are considered as ideal square planes, the Cu^{2+} ions form a diamond chain with identical Cu-O-Cu superexchange interactions and identical Cu-O···O-Cu super-superexchange interactions across the diagonal directions of each diamond. The reported magnetic susceptibility on $Bi_4Cu_3V_2O_{14}$ shows a characteristic feature of a low-dimensional antiferromagnet (AFM) with a broad maximum around 20.5 K. The specific heat, the ^{51}V NMR,[12] and the electron-spin-resonance measurements[13] show an antiferromagnetic spin ground state below around 6 K. Moreover, the high-field magnetization indicates a change in magnetic structure around 6.7 and 15 T. All these studies were performed on polycrystalline samples, though. Until now, no studies have been done on single crystals which we believe is crucial to confirm the existence of an antiferromagnetic long-ranged order as well as the metamagnetic transition in $Bi_4Cu_3V_2O_{14}$.

Therefore, here we report the magnetization, magnetic torque, specific-heat, and ^{51}V NMR measurements on a $Bi_4Cu_3V_2O_{14}$ single crystal with applied magnetic fields up to 35 T. For $H \| a$, we found a metamagnetic transition from an AFM to a weak-ferromagnetic (WFM) state at $H_c \simeq 7.6$ T below 5.5 K. Based on our magnetization data together with the ^{51}V NMR results at high magnetic fields we

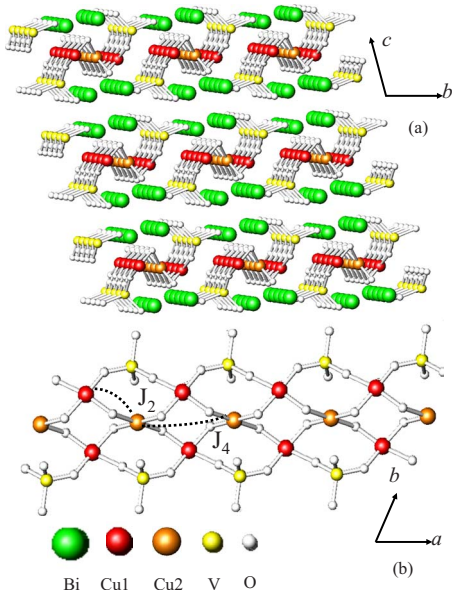

FIG. 1. (Color online) Structure of $Bi_4Cu_3V_2O_{14}$. (a) The projection of *bc* plane and (b) a chain structure along the *a* axis.

conclude that the spin structure is consistent with a canted antiferromagnetic one, with two distinct magnetic sublattices.

II. EXPERIMENT

A single crystal of $Bi_4Cu_3V_2O_{14}$ was grown by the traveling-solvent floating-zone technique. The feed and seed rods for the crystal growth were prepared by solid-state reaction. Appropriate mixtures of Bi_2O_3, CuO, and V_2O_5 were ground together and then calcined at 700 °C in air for 1 week. The mixture was then pressed into 6 mm×60 mm rods under 400 atm hydrostatic pressure and then calcined at 700 °C in air for 2 days. The rods were prescanned in the image furnace with a speed of 5 mm/h. After that, the crystal was grown with a speed of 0.5 mm/h. The powder x-ray diffraction pattern on the ground crystals shows a single $P\bar{1}$ structure for $Bi_4Cu_3V_2O_{14}$. Single-crystal x-ray diffraction data were collected on a Oxford Diffraction Xcalibur2 single-crystal x-ray diffractometer with Mo $K\alpha$ source at room temperature. The data was integrated by CRYSALIS and was corrected for absorption effects by Schwarzenbach psi method using scale3 abs correction in the same program. Space-group assignment was done by XPREP and the structure refinement was carried out using SHELXTL. The x-ray Laue diffraction was used to orient the crystal. dc-susceptibility measurements were made by a vibrating sample magnetometer. The magnetic torque data were measured by using a thin-film CuBe cantilever with thickness of 0.0125 mm. The specific-heat measurements were performed on a physical property measurement system (PPMS, Quantum Design). The field dependencies of the thermometer and addenda were carefully calibrated before specific-heat measurements. Both magnetic torque and specific heat were measured with applied magnetic fields along the a axis of the crystal. ^{51}V NMR experiments were completed down to 1.6 K on an oriented single crystal with external magnetic field applied along the a axis. The ^{51}V spectra were obtained by sweeping the magnetic field at fixed frequency.

III. RESULTS

The crystallographic data obtained at room temperature for the as-grown single crystals of $Bi_4Cu_3V_2O_{14}$ are shown in Table I. The data is consistent with the reported structural data.[14]

Figure 2(a) shows the temperature dependencies of the magnetic dc susceptibility (χ) with a field of 0.5 T applied both parallel and perpendicular to the a axis. χ exhibits a Curie-Weiss-type behavior at high temperatures. Above 50 K, the linear fit of $1/\chi$ with $H\|a$ yields a Curie-Weiss constant $\theta=-57$ K and an effective moment $\mu_{\text{eff}}=1.78\ \mu_B$, which is consistent with the μ_{eff} of Cu^{2+} ($S=1/2$). A broad peak appears around 24 K, which can be attributed to low-dimensional magnetic fluctuations. Below 5.5 K, χ drops down for $H\|a$ but goes up for $H\perp a$. The drop of χ_a at about 5.5 K reveals an AFM transition with staggered magnetization along the a axis. Figure 2(b) shows the field dependence of the magnetization (M) at 0.7 K for $H\|a$ and $H\perp a$. For

TABLE I. Crystallographic data for $Bi_4Cu_3V_2O_{14}$.

Space group	$P\bar{1}$ (No. 2)
a (Å)	5.3106(1)
b (Å)	7.9019(2)
c (Å)	8.0722(2)
α (deg)	74.038(2)
β (deg)	90.597(2)
γ (deg)	70.417(2)
V (Å^3)	306.573(12)
Z	1
ρ_{cal} (g/cm^3)	7.325
μ (mm^{-1})	63.80
Data collection range (deg)	$2.84<\theta<66.24$
Reflections collected	10863
Independent reflections	7441 [$R_{\text{int}}=0.1070$]
Parameter refined	107
R_1,[a] $wR_2[F_o>4\sigma F_o]$ [b]	0.0839, 0.1785
R_1,[a] wR_2 [b] (all data)	0.0679, 0.1741
Goodness of fit	1.002

[a] $R_1=\Sigma\|\|F_o\|-\|F_d\|\|/\Sigma|F_o|$.
[b] $wR_2=[\Sigma w(F_o^2-F_c^2)^2/\Sigma w(F_o^2)^2]^{1/2}$, $w=[\sigma^2(F_o)^2+(A\cdot p)^2+B\cdot p]^{-1}$, $p=(F_o^2+2F_c^2)/3$, $A=0.0067$, $B=0$.

$H\|a$, a rapid superlinear rise in $M_a(H)$ is observed around 7.6 T. This feature can be clearly seen from the dM_a/dH plot [Fig. 2(b)]. The appearance of a sharp peak in dM_a/dH is an indication of a phase transition and the peak position defines the critical field $H_c=7.6$ T. For $H\perp a$, the magnetization

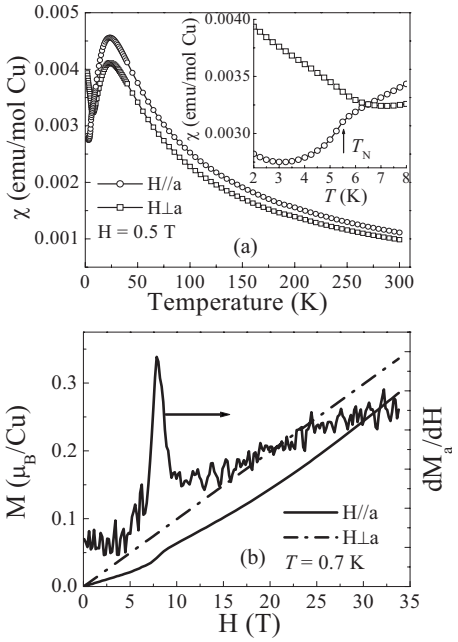

FIG. 2. (a) The temperature dependencies of the susceptibility for $H\|a$ and $H\perp a$. Inset: susceptibility at low temperatures; (b) the field dependencies of magnetization for $H\|a$ and $H\perp a$, and the $dM_a/dH\sim H$ curve.

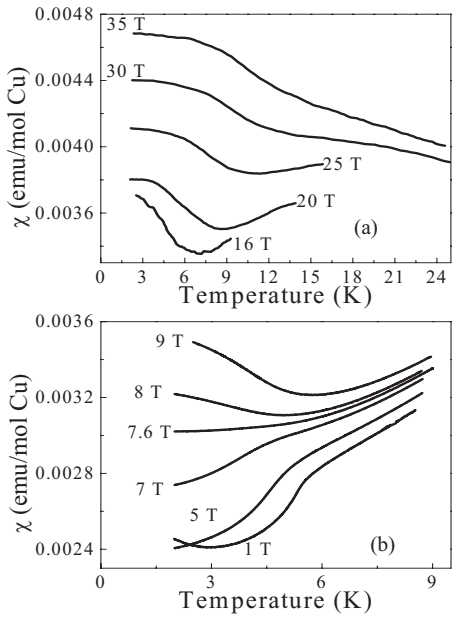

FIG. 3. The temperature dependencies of the susceptibility measured at different magnetic fields with $H \| a$ for $Bi_4Cu_3V_2O_{14}$ (a) $H > 9$ T and (b) $H \leq 9$ T.

shows a typical paramagnetic (PM) behavior, increasing linearly with H up to 35 T. This anisotropic magnetic response of the system suggests that the magnetic moments of the Cu ions are along the a axis. It is worth mentioning that, in contrast with previous reports on polycrystalline samples,[12] the $Bi_4Cu_3V_2O_{14}$ single crystal studied here allowed us to observe the anisotropic properties present in this system, although we found similar magnetic behavior.

Figure 3 shows the temperature dependencies of the susceptibility for different applied magnetic fields along a direction. With increasing field, the drop of χ decreases, suggesting that T_N is being suppressed. Actually, with $H=7.6$ T, the low-temperature χ becomes constant, and for $H>7.6$ T, χ begins to increase with decreasing temperature. At higher fields with $H \geq 20$ T, as shown in Fig. 3(a), χ increases with decreasing temperature and becomes flat below 4–5 K, which shows the tendency to a saturation at low temperatures. The peak position obtained from the $d\chi/dT$ curves shown in the Fig. 4 defines the magnetic transition temperature. With increasing field, the peak broadens and moves toward low temperature. For $H=7.6$ T, the $d\chi/dT$ curve shows no signature of peak above 2 K. With $H>7.6$ T, the peak inverts the sign and moves toward higher temperature with increasing field. The magnetic torque measurements also show different behavior from low fields to high fields. As shown in Fig. 5(a), at 0 T, the torque data shows a broad peak at low temperature, which position is consistent with the transition temperature obtained from the susceptibility data. At 18 T, the torque data shows a completely different behavior: it drops with decreasing temperature below 11 K. The peak observed on its derivative defines the transition temperature. Similar to the magnetization data, the field dependence of the magnetic torque also reveals a superlinear rise around $H_c=7.6$ T with a sharp peak on its derivative [see Fig. 5(b)].

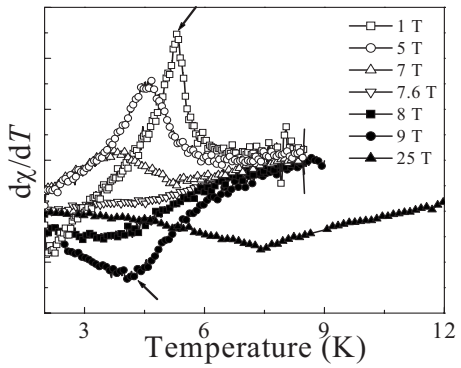

FIG. 4. The derivative of the susceptibility at several magnetic fields.

As shown in Fig. 6, the specific heat measured with $H \| a$ also indicates a magnetic transition at high magnetic fields. The specific heat shows a sharp peak at about 5.5 K at zero field, which corresponds to the magnetic ordering transition observed in the susceptibility measurements. With increasing field, the peak broadens and becomes weaker and its position, defining the transition temperature, decreases. Around 7 T, the data is very flat and the peak is almost unobservable. But with H above 9 T, a new broad peak shows up and moves toward higher temperatures, becoming stronger with increasing applied magnetic field. The inset of Fig. 6 shows the field dependence of the specific heat at 2.4 K with $H \| a$. At low fields, C_P increases with increasing field, but drops down after a maximum at around 8 T, quite consistent with

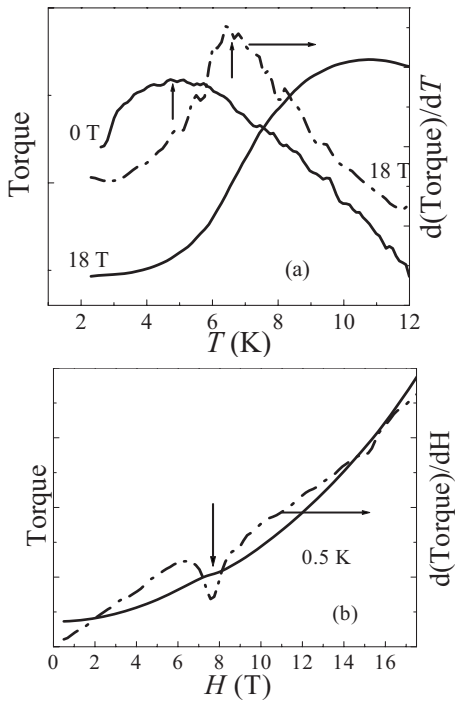

FIG. 5. (a) The temperature dependencies of the magnetic torque (solid lines) at $H=0$ and 18 T with $H \| a$, and the derivative of the magnetic torque (dashed-dotted line) at $H=18$ T; (b) the field dependence of the magnetic torque (solid line) measured at 0.5 K and its derivative (dashed-dotted line).

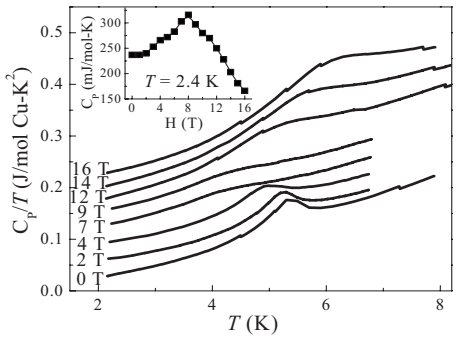

FIG. 6. The temperature dependencies of C_P/T at different magnetic fields with $H\|a$ of $Bi_4Cu_3V_2O_{14}$. Each curve of C_P/T is manually shifted up by 0.03 J/mol Cu K^2 with increasing magnetic field from 0 T to show the data more clearly. Inset: the field dependence of C_P measured at 2.4 K.

the transition at $H_c \simeq 7.6$ T observed on the susceptibility and magnetic torque data.

The field-swept ^{51}V NMR spectra measured with the magnetic field along the a axis are shown in Figs. 7 and 8. Figure 7 shows the spectra measured at fields $H^{\|a} \simeq 3.96$ T and fixed frequency $\nu = 45.1$ MHz above and below $T_N \simeq 5.5$ K in the low-field region of the phase diagram displayed in Fig. 10. The single NMR line observed in the PM state clearly splits symmetrically into two lines below T_N. From the splitting of the lines we directly estimate the internal field H_{int} generated at the ^{51}V sites by the Cu(1) and Cu(2) moments when $H\|a$. We found that $H_{int}^{\|a} \simeq 0.17$ T.

We have also carried out NMR experiments in the high-field region of the phase diagram with $H > H_c = 7.6$ T along the a axis. Figure 8 presents the field-swept ^{51}V NMR spectra measured at fields $H^{\|a} \simeq 11.8$ T and fixed frequency $\nu = 133.78$ MHz. The single line observed in the PM state ($T > 8$ K) clearly splits into four distinct peaks. As inferred from the fits of the spectra, we were able to identify two sets of split lines with different H_{int} along with a broad background peak for $T \leq T_N \simeq 6.1$ K. We found $H_{int}(1) \simeq 0.04$ T for the inner set of split lines and $H_{int}(2) \simeq 0.10$ T for the outer ones at the lowest measured temperature $T = 1.6$ K. The temperature dependence of $H_{int}(1)$ and $H_{int}(2)$ are shown in Fig. 9. The solid (red) lines are the best fit to the magnetic order parameter $M(T) = M_0[1 - (T/T_N)]^\alpha$ (molecular field theory) with the parameters $M_0(1) = 0.041(2)$ T, $M_0(2) = 0.105(3)$ T, $T_N = 6.1$ K, and $\alpha = 0.1$.[15] The inset of Fig. 9 presents the position of the ^{51}V NMR line as a function of temperature. Below $T_N = 6.1$ K the data indicates the middle point of the split spectra moves toward lower fields with decreasing temperature. It is worth mentioning that the middle point of the two distinct set of split spectra as well as the broad peak coincide for all temperatures as inferred from Fig. 8.

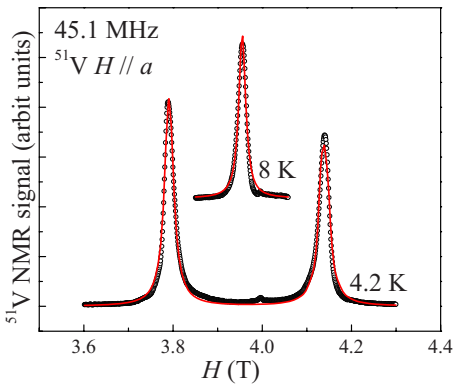

FIG. 7. (Color online) Field-swept ^{51}V NMR spectra measured with $H^{\|a} \simeq 3.96$ T at fixed frequency $\nu = 45.1$ MHz above and below $T_N \simeq 5.5$ K. The open circles are experimental data and the solid (red) lines are fits using Lorentzian lines.

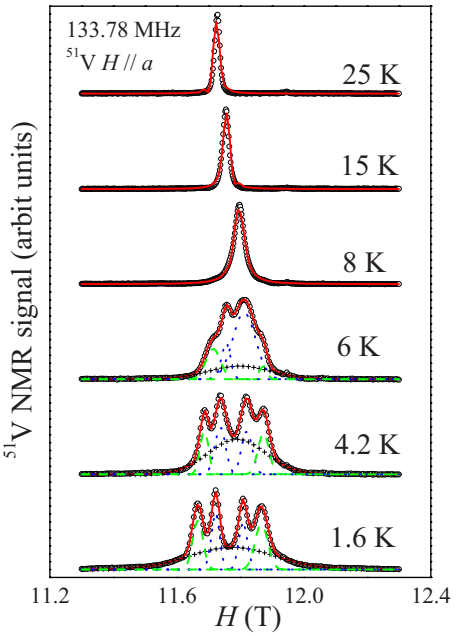

FIG. 8. (Color online) Field-swept ^{51}V NMR spectra as a function of temperature measured with $H^{\|a} \simeq 11.8$ T at fixed frequency $\nu = 133.78$ MHz. The open circles are experimental data and the solid (red) lines are fits of the full spectra using Lorentzian lines. The dotted (blue) and dashed (green) lines indicate the two distinct sets of split spectra. The crosses indicate the broad background.

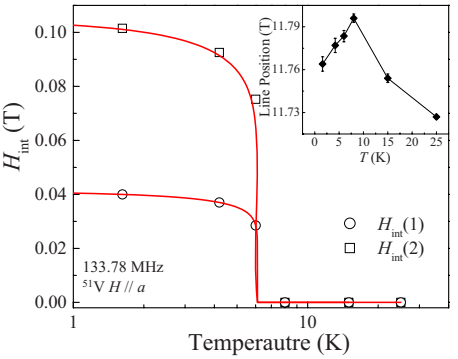

FIG. 9. (Color online) Temperature dependence of $H_{int}(1)$ and $H_{int}(2)$ with $H^{\|a} \simeq 11.8$ T. The open symbols are experimental data and the solid (red) lines are best fits using the temperature dependence of the magnetic order parameter $M(T)$ described in the text. Inset: T dependence of the position of the lines from Fig. 8.

IV. DISCUSSION

The above results clearly show that there is a metamagnetic transition around $H_c \simeq 7.6$ T at low temperatures. The susceptibility data show that the AFM transition below 5.5 K is suppressed to low temperatures with increasing field. Above $H_c \simeq 7.6$ T, a new magnetic phase develops and its transition temperature increases with increasing field. The tendency of the susceptibility to saturate at high magnetic fields and low temperatures suggests the presence of a FM component in the system. Thus, based on our results, this metamagnetic transition is probably a consequence of a spin-flop transition from an AFM to a WFM state.

The applied magnetic field usually suppresses the AFM correlations as well as the transition temperature through a magnetic transition from PM to AFM. However, when the transition is from a PM to a WFM state, the transition temperature is expected to increase with increasing fields, since the WFM correlations are enhanced. Our specific-heat data indicate that the magnetic ordering is indeed AFM like at low fields, but WFM like at high fields, quite consistent with the susceptibility measurements. The increase in C_P at low fields may be understood by assuming a field-induced enhancement of the spin density of states. The magnetic specific heat at low temperatures is proportional to the total density of the low-lying excitations. The applied field suppresses the AFM coupling and then enhances the density of spin excitations. Above $H_c \simeq 7.6$ T, a transition to a ferromagnetically polarized state occurs and C_P decreases with further increasing field. When the field is large enough to polarize the whole spin system, the spin excitations are completely suppressed and no longer have contribution to the specific heat.

The ^{51}V NMR spectra provide further information about this scenario of $Bi_4Cu_3V_2O_{14}$. When the temperature is lowered below T_N=5.5 K, the NMR spectrum splits, doubling the number of resonance lines when $H^{\|a} \simeq 3.96$ T (Fig. 7). This is a microscopic evidence that the sample undergoes an AFM transition, consistent with the results found for the magnetic dc-susceptibility, torque, and specific-heat experiments. The AFM moments generate a spontaneous internal hyperfine field (H_{int}) proportional to the split of the lines in the ordered state. In the crystal structure, there are two distinct Cu sites along the a axis, as shown in Fig. 1(b). The V ions are connected to the Cu(1) ions by oxygen bonds but not connected to the Cu(2) ions. The symmetric splitting of the lines when $H \| a \simeq 3.96$ T indicates that the Cu(1) and Cu(2) sites are equivalent since the lines remain relatively narrow below the transition. It also suggests that the main component of H_{int} generated by the Cu moments at the ^{51}V sites is along the a axis since $H_{eff}=H \pm H_{int}$. This is in agreement with the magnetization data which also suggest resultant Cu moments arranged AFM along the a axis (easy axis). The theoretical calculation[16] shows that the ground state of $Bi_4Cu_3V_2O_{14}$ is a AFM phase dominated by the superexchange interaction J_2 coupled through the super-superexchange interaction J_4, as shown in Fig. 1(b). This is consistent with the results shown here.

The internal field is also estimated by considering the Cu moment given in Fig. 2. For $H^{\|a} \simeq 3.96$ T, the Cu moment is only about $M \sim 0.017$ μ_B/Cu. The nearest-neighbors Cu is located at a distance of 3.27 Å from the V ions. A simple calculation considering only dipolar fields from the Cu moments at the V site gives an upper limit of $H_{int} \sim 9$ Oe. This is definitely too small compared to our experimental observation of $H_{int} \sim 0.17$ T (Fig. 7) and definitely indicates that the case here must be more complicated. Indeed, the underlying physics in $Bi_4Cu_3V_2O_{14}$ involve not only dipolar fields but also transferred hyperfine fields, which must also be a very important contribution to be considered.

For $H^{\|a} > 7.6$ T, the NMR spectrum also splits below T_N. Nonetheless, the split is twofold as shown in Fig. 8, suggesting the emergence of two different magnetic sublattices. The two distinct and smaller values of H_{int} [$H_{int}(1) \simeq 0.041$ T and $H_{int}(2) \simeq 0.105$ T] suggest that after the spin-flop transition at $H_c \simeq 7.6$ T, the Cu(1) and Cu(2) sites are no longer equivalent to the ^{51}V ions and, thus, their magnetic moments generate two distinct AFM sublattices. One plausible scenario to explain such observation is that the magnetostriction caused by the spin-flop transition could indeed distort the structure along the a axis and lead to nonequivalent Cu sites with relation to the ^{51}V ions.

From the fits in Fig. 9 we obtained α=0.1. The fact that α is smaller than 0.5, the value expected for the three-dimensional mean field, suggests that the reduced value may be due to the chain structure or the low-dimensional magnetic structure of $Bi_4Cu_3V_2O_{14}$. Furthermore, the broad background peak shown in Fig. 8 either indicates that the magnetic structure is changing with increasing field (canting the moments) or the magnetic ordering becomes incommensurate. The observed magnetic shift of the lines toward lower fields below $T_N \simeq 6.1$ K suggests the presence of a weak FM. In order to obtain weak ferromagnetism along the a axis after the spin-flop transition, the flopped spins would have to rearrange with a *canted* angle in relation to the a axis. The NMR data presented here do provide further microscopic evidences of the magnetic ordering temperatures as well as the presence of a WFM component for $H \geq H_c$=7.6 T as suggested by the bulk measurements. In the high-field phase, the increase in the transition temperature, the decrease in the specific-heat value, the shift of the spectra toward low fields with increasing fields, along with the saturation of the susceptibility, strongly indicate the existence of weak FM. How-

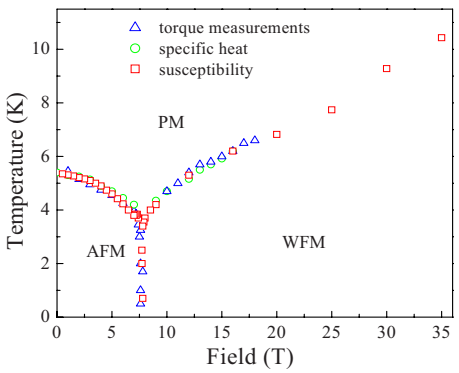

FIG. 10. (Color online) The magnetic phase diagram of $Bi_4Cu_3V_2O_{14}$. PM, AFM, and WFM represent a paramagnetic, an antiferromagnetic, and a weak-ferromagnetic phases, respectively.

ever, in order to confirm the magnetic structure in this system further NMR experiments with H along the other crystallographic axes b and c would be required but this is not the scope of the present study.

Finally, based on the magnetic and specific-heat data, we propose a low-temperature magnetic phase diagram for $Bi_4Cu_3V_2O_{14}$ in Fig. 10. At higher temperatures, $Bi_4Cu_3V_2O_{14}$ is in a Curie-Weiss-type paramagnetic phase. By lowering the temperature, it falls into either, an AFM phase in the low-field region of the phase diagram with $H \lesssim H_c = 7.6$ T, or, into a WFM phase in the high-field region of the phase diagram with $H \gtrsim H_c = 7.6$ T. The AFM phase is therefore connected with the ferromagnetically polarized phase by a spin-flop transition at $H_c = 7.6$ T.

In summary, single crystals of $Bi_4Cu_3V_2O_{14}$ have been successfully grown by floating-zone technique. The magnetic properties reported here with $H \| a$ show a metamagnetic transition from antiferromagnetism to weak ferromagnetism observed at $H_c = 7.6$ T. The NMR results provide further evidence for the proposed phase diagram and suggest that the weak ferromagnetism observed for $H > H_c = 7.6$ T is probably a consequence of a canted antiferromagnetic spin structure with two distinct magnetic sublattices. Nevertheless, further microscopic studies, such as NMR and neutron-diffraction experiments, would provide strong support in order to obtain more details and establish the actual spin structure of this system.

ACKNOWLEDGMENTS

This work utilized facilities supported in part by the NSF through the Cooperative Agreement No. DMR-0654118 and the State of Florida. Tozer acknowledges the National Nuclear Security Administration under the Stewardship Science Academic Alliances program through DOE under Grant No. DE-FG52-10NA29659. Wiebe acknowledges NSERC program.

*zhou@magnet.fsu.edu

[1] M. Hase, I. Terasaki, and K. Uchinokura, Phys. Rev. Lett. **70**, 3651 (1993).
[2] M. Jaime, V. F. Correa, N. Harrison, C. D. Batista, N. Kawashima, Y. Kazuma, G. A. Jorge, R. Stein, I. Heinmaa, S. A. Zvyagin, Y. Sasago, and K. Uchinokura, Phys. Rev. Lett. **93**, 087203 (2004).
[3] M. Azuma, Z. Hiroi, M. Takano, K. Ishida, and Y. Kitaoka, Phys. Rev. Lett. **73**, 3463 (1994).
[4] N. Kobayashi, Z. Hiroi, and M. Takano, J. Solid State Chem. **132**, 274 (1997).
[5] Z. He, T. Kyomen, and M. Itoh, Phys. Rev. B **69**, 220407 (2004).
[6] I. Tsukada, J. Takeya, T. Masuda, and K. Uchinokura, Phys. Rev. Lett. **87**, 127203 (2001).
[7] M. Baenitz, C. Geibel, M. Dischner, G. Sparn, F. Steglich, H. H. Otto, M. Meibohm, and A. A. Gippius, Phys. Rev. B **62**, 12201 (2000).
[8] Z. He and Y. Ueda, Phys. Rev. B **77**, 052402 (2008).
[9] A. N. Vasil'ev, L. A. Ponomarenko, H. Manaka, I. Yamada, M. Isobe, and Y. Ueda, Phys. Rev. B **64**, 024419 (2001).
[10] A. V. Prokofiev, I. G. Vasilyeva, V. N. Ikorskii, V. V. Malakhov, I. P. Asanov, and W. Assmus, J. Solid State Chem. **177**, 3131 (2004).
[11] M. G. Banks, F. H. meisner, A. Honecker, H. Rakoto, J. M. Broto, and R. K. Kremer, J. Phys.: Condens. Matter **19**, 145227 (2007).
[12] H. Sakurai, K. Yoshimura, K. Kosuge, N. Tsujii, H. Abe, H. Kitazawa, G. Kido, H. Michor, and G. Hilscher, J. Phys. Soc. Jpn. **71**, 1161 (2002).
[13] S. Okubo, T. Hirano, Y. Inagaki, H. Ohta, H. Sakurai, H. Yoshimura, and K. Kosuge, Physica B **346-347**, 65 (2004).
[14] G. B. Deacon, B. M. Gatehouse, and G. N. Ward, Acta Crystallogr., Sect. C: Cryst. Struct. Commun. **50**, 1178 (1994).
[15] T. Moriya, *Spin Fluctuations in Itinerant Electron Magnetism* (Springer-Verlag, Berlin, 1985).
[16] H. J. Koo and M. H. Whangbo, Inorg. Chem. **47**, 4779 (2008).